Article:

Rosentreter, JA, Laruelle, GG, Bange, HW et al. (12 more authors) (2023) Coastal vegetation and estuaries are collectively a greenhouse gas sink. Nature Climate Change, 13 (6). pp. 579-587. ISSN 1758-678X

https://doi.org/10.1038/s41558-023-01682-9

Title: Coastal vegetation and estuaries collectively are a greenhouse gas sink

Author list: Judith A. Rosentreter[1,2,3*], Goulven G. Laruelle[4], Hermann W. Bange[5], Thomas S. Bianchi[6], Julius J. M. Busecke[7], Wei-Jun Cai[8], Bradley D. Eyre[1], Inke Forbrich[9,10], Eun Young Kwon[11], Taylor Maavara[2,3,12], Nils Moosdorf[13,14,15], Raymond G. Najjar[16], V.V.S.S. Sarma[17], Bryce Van Dam[18], Pierre Regnier[4]

Affiliations:

[1]Center for Coastal Biogeochemistry, Faculty of Science and Engineering, Southern Cross University, Lismore, Australia

[2]Yale Institute for Biospheric Studies, Yale University, New Haven, USA

[3]Yale School of the Environment, Yale University, New Haven, USA

[4]Biogeochemistry and Modelling of the Earth System-BGEOSYS, Department of Geoscience, Environment and Society, Université Libre de Bruxelles, Brussels, Belgium

[5]Marine Biogeochemistry, Helmholtz Centre for Ocean Research Kiel, Kiel, Germany

[6]Department of Geological Sciences, University of Florida, Gainesville, USA

[7]Lamont-Doherty Earth Observatory of Columbia University, Palisades, New York, USA

[8]School of Marine Science and Policy, University of Delaware, Newark, DE, USA

[9]Ecosystems Center, Marine Biological Laboratory, Woods Hole, USA

[10]Department of Environmental Sciences, University of Toledo, Toledo, USA

[11]Center for Climate Physics, Institute for Basic Science, Busan, South Korea

[12]School of Geography, University of Leeds, United Kingdom

[13]Leibniz Centre for Tropical Marine Research (ZMT), Bremen, Germany

[14]Kiel University, Kiel, Germany

[15]Southern Cross Geoscience, Southern Cross University, Lismore, Australia

[16]Department of Meteorology and Atmospheric Science, The Pennsylvania State University, University Park, PA, USA

[17]CSIR-National Institute of Oceanography, 176 Lawsons Bay Colony, Visakhapatnam, India

[18]Department of Fluxes across interfaces, Institute of carbon cycles, Helmholtz-Zentrum Hereon, Geesthacht, Germany

*email: judith.rosentreter@scu.edu.au

Abstract:

Coastal ecosystems release or absorb carbon dioxide (CO_2), methane (CH_4), and nitrous oxide (N_2O), but the net effects of these ecosystems on the radiative balance remain unknown. We compiled a dataset of observations from 738 sites from studies published between 1975 and 2020 to quantify CO_2, CH_4, and N_2O fluxes in estuaries and coastal vegetation in ten global regions. We show that the CO_2-equivalent (CO_2e) uptake by coastal vegetation is reduced by 23-27% due to estuarine CO_2e outgassing, resulting in a global median net sink of 391 or 444 Tg CO_2e yr^{-1} using the 20 or 100-year global warming potential, respectively. Globally, total coastal CH_4 and N_2O emissions reduce the coastal CO_2 sink by 9-20%. Southeast Asia, North America, and Africa are critical regional hotspots of greenhouse gas sinks. Understanding these hotspots can guide our efforts to strengthen coastal CO_2 uptake while effectively reducing CH_4 and N_2O emissions.

Keywords: Coastal vegetation, estuaries, climate change, greenhouse gas budget, radiative balance

Main text:

Since the beginning of the industrial era, atmospheric concentrations of the greenhouse gases (GHG) CO_2, CH_4, and N_2O have increased by 47%, 156% and 23%, respectively, and continue to increase at alarming rates due to anthropogenic activities, driving global warming[1]. The global terrestrial CO_2 sink is diminished by biogenic CH_4 and N_2O emissions due to anthropogenic activities such as agriculture or biomass burning, which resulted in a shift of the terrestrial biosphere from a net CO_2 sink to a net GHG source[2]. Globally, it is now clear that inland waters are an atmospheric GHG source[3,4] while the GHG budget of coastal ecosystems is less certain. Located in the downstream portion of the Land-Ocean-Aquatic-Continuum (LOAC)[5], estuaries receive large amounts of terrestrial carbon (C) and nitrogen (N) through riverine and groundwater flows, but their C and N cycles are also tightly inter-connected with coastal vegetated ecosystems[6] and the coastal oceans[7,8]. The GHG radiative balance of estuaries and coastal vegetation are thus a complex spatial and temporal combination of GHG sources and sinks[7], which complicates the estimate of the net global warming effect and makes the implementation of efficient mitigation strategies difficult.

Estuaries (tidal systems and deltas, lagoons, fjords) and surrounding coastal vegetation (mangroves, salt marshes, seagrasses) are strongly interconnected but show remarkable variations in the magnitude and direction (sink or source) of GHG fluxes. Estuaries have been estimated to emit 0.4 to 2.2 Pg CO_2 yr^{-1} globally[7–10], whereas mangroves and salt marshes collectively take up 0.3 to 1.7 Pg CO_2 yr^{-1} [5,8] (Supplementary Table S1). Together with submergent seagrasses, coastal vegetation potentially store 304 (131-466) Tg CO_2 yr^{-1} of so-called 'blue carbon' in their sediments[11,12]. On the other hand, emissions of CH_4 and N_2O from coastal sediments and surrounding waters can reduce some of the coastal vegetation carbon sinks[13,14], thereby complicating 'blue carbon' assessments[15,16]. A recent global synthesis showed that median CH_4 emissions from combined mangrove, salt marshes, and seagrasses (0.52 Tg CH_4 yr^{-1}) exceed those from estuaries (0.23 Tg CH_4 yr^{-1})[17]. However, CH_4 fluxes are highly variable across time and space, causing a large range in global estimates of both coastal vegetation (0.02 to 6.2 Tg CH_4 yr^{-1})[17,18] and estuaries (0.02 to 6.6 Tg CH_4 yr^{-1})[4,19] (Supplementary Table S2). Coastal N_2O fluxes are less understood and it remains unclear if coastal vegetated ecosystems are a net source or sink of N_2O to the atmosphere[20,21]. Global estimates of estuarine N_2O emissions are highly uncertain, with large discrepancies for both observation-based (110 to 2,844 Gg N_2O yr^{-1})[4,22,23] and modeling (94 to 1,084 Gg N_2O yr^{-1})[24,25] approaches (Supplementary Table S3).

Here we present a data-driven meta-analysis synthesizing CO_2, CH_4, and N_2O fluxes in three major estuary types (tidal systems and deltas, lagoons, and fjords) and three coastal vegetation types (mangroves, salt marshes, seagrasses), globally and in ten world regions. These regions were delineated by the REgional Carbon Cycle Assessment and Processes-2 (RECCAP2) project[26], an activity of the Global Carbon Project. We compiled water-air CO_2, CH_4, and N_2O fluxes for estuaries and combined CO_2 fluxes from eddy-covariance with CH_4 and N_2O fluxes at the interfaces of water, sediments, and plants with the atmosphere for coastal vegetation. Our dataset compiles observations from a total of 738 sites from studies published between 1975 and end of 2020 and we provide a GHG flux climatology assumed representative for this period. The GHG fluxes are regionalized by combining GHG flux densities with recently published surface areas of coastal vegetation[27–29] and estuaries[30]. As such, our global-scale regional assessment applies a consistent framework for all three GHGs and ecosystems. Regional GHG fluxes are then summed to provide global net GHG fluxes for estuaries, coastal vegetation, and both systems combined. We quantify the net contemporary GHG radiative balance in units of CO_2-equivalents (CO_2e) based on the global warming potential (GWP) of each gas for the 20-year and 100-year time horizons[1]. Note that our study does not include an analysis of temporal changes in GHG fluxes required to assess a contribution to radiative forcing. Following the RECCAP2 regional segmentation, our coastal GHG budget can be integrated into broader budgets of continents.

Estuarine and coastal vegetation CO_2 fluxes

We estimate global median [first (Q1)-third (Q3) quartile] CO_2 emissions from estuaries at 111 [73-170] Tg CO_2 yr^{-1} (Table 1), which is three to five times lower (as is our mean of 121 Tg CO_2 yr^{-1}) than recent mean estimates (370-550 Tg CO_2 yr^{-1})[9,10]. Our lower global emissions are due to the inclusion of estuarine surface area[30] (Extended Data Figure 1) that is ~30% lower than previously estimated[31,32], and includes more sites than previous studies[9,10]. In particular, CO_2 flux data in fjords have more than doubled since earlier reviews[8,10] that considered fjords as minimal CO_2 sources. Here we show that fjords take up 66 [96-24] Tg CO_2 yr^{-1} from the atmosphere, reducing 37% of the CO_2 emissions from global tidal systems and deltas (127 [90-176] Tg CO_2 yr^{-1}) and lagoons (50 [28-81] Tg CO_2 yr^{-1}) (Figure 1). Tidal systems and deltas which account for 40% of the global estuarine surface area (Supplementary Table S4) show higher CO_2 flux densities than lagoon and fjords (Supplementary Table S5), likely due to their strong hydrological connectivity with rivers and groundwater that import CO_2 supersaturated waters[33]. In addition, the considerably strong influence by tides[31] can increase water turbulence and therefore gas transfer velocities[34] which in turn enhance CO_2 evasion from tidal systems. At the regional scale, we find distinct trends of CO_2 fluxes between different geomorphic estuary types (Figure 1). For example, North America is a hotspot for atmospheric CO_2 uptake by fjords (57 [76-30] Tg CO_2 yr^{-1}, 86% of the CO_2 uptake by global fjords). Long stretches of lagoons can be found along Africa's coastline that contribute 24% to global lagoon CO_2 emissions. Europe accounts for 20% of global CO_2 emissions by tidal systems and deltas although only comprising 5% of the total surface area of this estuary type. This disproportionate contribution stems from the highest median CO_2 flux densities (4.7 g CO_2 m^{-2} d^{-1}) of any estuary type or region (Supplementary Table S5), likely fuelled by organic carbon loads from European rivers under strong anthropogenic pressure[35]. European estuaries were over-represented in previous global analyses[9,10,36], which likely led to overestimates in global CO_2 emissions from estuaries.

Using data exclusively from eddy-covariance long-term studies, we estimate that salt marshes, mangroves, and seagrasses worldwide take up 601 [774-426] Tg CO_2 yr^{-1} from the atmosphere, a flux which, in absolute terms, is more than five times greater than the estuarine CO_2 outgassing (Table 1). Our global estimate is lower but within the uncertainty range of a recent estimate of 843±440 Tg CO_2 yr^{-1} by mangroves, salt marshes, and seagrasses[5]. Note that our estimate of CO_2 uptake by coastal vegetation should be distinguished from carbon sequestration by coastal vegetation, which has been estimated to be 110-257 Tg CO_2 yr^{-1} [37], roughly ⅓ of the CO_2 uptake, the remainder resulting in a lateral export of carbon, a substantial fraction of which can be transported over long distances to the open ocean[5].

Seagrass meadows can be found in tropical, subtropical, and temperate-cold climate zones. Mangroves are only abundant in subtropical and tropical climates, whereas salt marshes dominate in temperate regions (Extended Data Figure 1, Extended Data Figure 2). Highly productive mangrove forests[38] contribute the majority (60%) of the global CO_2 uptake by coastal vegetation (359 [434-333] Tg CO_2 yr^{-1}). Globally, seagrasses (192 [354-53] Tg CO_2 yr^{-1}) have a ~4 times higher CO_2 uptake than salt marshes (50 [59-41] Tg CO_2 yr^{-1}) (Figure 2), which is similar to previous findings based on net primary production[39]. Since mangrove forests are abundant in tropical southeast Asia, we find that this region contributes 37% to global mangrove CO_2 uptake, followed by Africa (20%), and tropical North and South America (both ~15%). Salt marshes are abundant along the west and east coasts of Canada and the US. Therefore, North America contributes 34% of the global salt marsh CO_2 uptake. Other regions that provide a substantial salt marsh CO_2 sink include East Asia (23%) and Australasia (21%). Africa's coastline has the greatest contribution (24%) to global seagrass CO_2 uptake.

Estuarine and coastal vegetation CH_4 fluxes

Global estuaries emit 0.25 [0.07-0.46] Tg CH_4 yr^{-1} (Table 1), a median value that falls at the lower end of the range of previous assessments[4,19,40] (Supplementary Table S2), yet is close to the recent median estimate (0.23 [0.02-0.91] Tg CH_4 yr^{-1}) by Rosentreter et al.[17]. Global estuarine CH_4 emissions are dominated by tidal systems and deltas (0.14 [0.11-0.23] Tg CH_4 yr^{-1}, 56%), and lagoons (0.11 [0.05-0.13] Tg CH_4 yr^{-1}, 44%), while fjords contribute <1%. Our regional analysis shows that North America's tidal systems and deltas contribute the majority (50%) of global CH_4 emissions from this estuary type (Figure 1). North America also shows the highest median CH_4 flux densities (2.9 mg CH_4 m^{-2} d^{-1}) of tidal systems and deltas, particularly in the USA, where many eutrophic systems undergo seasonal hypoxia or anoxia that fuel CH_4 production[41]. South America, Russia, and Australasia contribute around 10% each to global CH_4 emissions from tidal systems and deltas, whereas all other regions are minor contributors (<5%). North America comprises the largest area of lagoons (Extended Data Figure 1), thereby dominating global lagoonal CH_4 emissions (30%). Other regions with substantial lagoon CH_4 emissions are Africa (25%) and South America (14%), whereas the remaining regions contribute <10%. Interestingly, we find that of all estuary types and regions, lagoons in Africa show the highest flux density (5.3 mg CH_4 m^{-2} d^{-1}), driven by high CH_4 production in anoxic bottom waters in permanently stratified lagoons along the Ivory Coast[42].

Globally, mangroves, salt marshes, and seagrasses combined release 0.76 [0.47-1.41] Tg CH_4 yr^{-1} which is more than three times the CH_4 released by global estuaries. Our coastal vegetation estimate is comparable with a recent review[17] but incorporates more data, which results in an increased estimate for salt marshes and mangroves but not seagrasses. We find that mangroves (0.34 [0.21-0.50] Tg CH_4 yr^{-1}) dominate coastal vegetation CH_4 emissions, followed by salt marshes (0.26 [0.14-0.36] Tg CH_4 yr^{-1}), and seagrasses (0.17 [0.09-0.21] Tg CH_4 yr^{-1}) (Table 1, Figure 2). The high CH_4 emissions from mangroves (exceeding global estuaries) are promoted by carbon-rich deep anoxic sediments[43] and by tidally induced mixing between groundwater rich in CH_4 and surface waters[44]. We find highest mangrove CH_4 flux densities (21 mg CH_4 m^{-2} d^{-1}) in East Asia. However, North America's mangrove forests dominate (41%) global mangrove CH_4 emissions because its forest area is 86 times greater than in East Asia and the CH_4 flux density is similarly high (Supplementary Table S6). Globally, Southeast Asia comprises most mangrove forest area, but the region's much lower CH_4 flux density (1.4 mg CH_4 m^{-2} d^{-1}) means that it adds only 6% to global mangrove CH_4 emissions. Such a low regional evasion rate may be explained by high monsoonal rainfall events and short water residence times, resulting in low rates of anaerobic organic matter decomposition[45]. The highest median CH_4 flux densities of any coastal vegetation type are found in East Asian salt marshes (44 mg CH_4 m^{-2} d^{-1}), with this region contributing 34% of global salt marsh CH_4 emissions despite its relatively small marsh coverage. North America's vast salt marsh areas are the second highest contributor (35%) to global salt marsh emissions. Australasia's seagrass meadows dominate (29%) global seagrass CH_4 emissions, a combination of moderately high seagrass area and a regional flux density that is more than twice the global median (Supplementary Table S6).

Estuarine and coastal vegetation N_2O fluxes

We estimate that estuaries globally emit 61 [41-94] Gg N_2O yr^{-1} (Table 1), which is substantially lower than previous observational and modeling estimates (94 to 5,710 Gg N_2O yr^{-1})[4,24,25,46] (Supplementary Table S3). Similar to CO_2 and CH_4, our lower estuary N_2O emissions are partially due to lower estuarine surface area used in this study[30], but also reflects the ~80% more sites in our analysis than earlier reviews[23,46]. We find the highest N_2O emissions in tidal systems and deltas (35 [24-48 Gg N_2O yr^{-1}), but in contrast to CO_2 and CH_4, fjords are the second highest N_2O emitters (16 [12-21] Gg N_2O yr^{-1}), almost double of those of lagoons (10 [6-14] Gg N_2O yr^{-1}). Regionally, North America contributes 27%, 37%, and 77% to global emissions from tidal systems and deltas, lagoons, and fjords, respectively, contributing 25 [17-33] Gg N_2O yr^{-1} (41%) to global estuary N_2O emissions (Figure 1). Other regions of moderate emissions are South America (14%), Russia (12%), and Southeast Asia (9%), with the remaining regions being only minor contributors (< 5 Gg N_2O yr^{-1}). We further compare our data-driven approach with the recently published mechanistic model of global estuary N_2O emissions[25] that was regionalised for comparison purposes. The modelled global emission estimates from all three estuary types (94 Gg N_2O yr^{-1}) fall close to the upper uncertainty bound reported in our study. As such, we find an overall good agreement between the two approaches. Fjord emissions represent the largest relative difference between modelled and data-driven estimates (Table 1).

Coastal vegetation can be sources or sinks of N_2O to the atmosphere. We find that emissions slightly exceed uptake at the global scale, resulting in 6.3 [0.7-18.3] Gg N_2O yr^{-1} which is only about 10% of the estuarine emission (Table 1). Globally, mangroves emit 8.8 [4.4-19.3] Gg N_2O yr^{-1}, more than four times than salt marshes (2.1 [-0.8-6.1] Gg N_2O yr^{-1}). Seagrasses take up 4.6 [6.0-3.4] Gg N_2O yr^{-1}, thereby offsetting almost half of the N_2O emitted by salt marshes and mangroves (Figure 2). Nevertheless, large variability can be found in local N_2O fluxes in coastal vegetation. For example, current studies report N_2O uptake from salt marshes in North America[47] and Europe[48], while studies from East Asia, mainly China, reveal that this region accounts for a substantial 1.3 [0.2-2.8] Gg N_2O yr^{-1} (62%) of global salt marsh emissions. Mangroves ecosystems are generally a source of N_2O although some mangrove creeks in Australia have been shown to consume N_2O due to low nitrogen concentrations[20,21]. Our seagrass N_2O flux database is strongly biased towards data from Australia, where studies mostly suggest N_2O uptake from near-pristine seagrasses[49] (Supplementary Table S7).

Implication for regional and global budgets

Our data-driven meta-analysis reveals that estuarine CO_2-equivalent GHG emissions reduce the coastal vegetation CO_2-equivalent GHG uptake, by 27% using the GWP_{20} and 23% using the GWP_{100}. Estuaries and coastal vegetation therefore are collectively a GHG sink for the atmosphere of 391 [647-76] Tg CO_2e yr^{-1} or 444 [675-175] Tg CO_2e yr^{-1} based on the GWP_{20} or GWP_{100}, respectively (Table 2, Figure 3). Our quantification of the net GHG sink is broadly consistent with previous assessments based solely on CO_2[5,7,8]. However, we find that this sink results both from a downward revision of coastal vegetation CO_2 fixation and substantially lower estuarine GHG outgassing, mostly due to the CO_2 uptake by fjords and a reduced estuarine surface area[30]. The net CO_2 sink of estuaries and coastal vegetation is also significantly compensated by CH_4 and N_2O emissions, which offset 20% and 9% for the GWP_{20} and GWP_{100}, respectively. Our global-scale assessment considerably reduces the uncertainty in the contemporary GHG budget[5] and emphasises that the combined contribution of coastal vegetation and estuaries on the global radiative balance is a cooling effect (Figure 4), in contrast to terrestrial sources[2] and inland waters[3,4]. However, our analysis does not address whether human activity has changed the radiative balance of these systems since the pre-industrial period. Importantly, we reveal where estuarine fluxes enhance, partially reduce, or exceed coastal vegetation CO_2 uptake, allowing us to identify regional hotspots of GHG uptake and release (Figure 3). We find that 8 out of 10 coastal regions are a net GHG sink for the atmosphere, regardless of the time horizon considered (Table 2). Using the GWP_{100}, Southeast Asia shows the greatest net GHG sink (156 [224-106] Tg CO_2e yr^{-1}) because of its extensive and highly productive tropical mangrove forests and seagrass meadows (Extended

Data Figure 1), as well as accommodating relatively few estuaries compared to other regions[30]. A second regional hotspot for GHG sinks is North America (128 [165-77] Tg CO_2e yr^{-1}) due to its expansive mangrove, salt marsh, and seagrass areas, while also hosting the largest area of CO_2-absorbing fjords globally (40% of which are located in Greenland). In Africa, the large CO_2 uptake by coastal vegetation is partially offset by estuarine GHG outgassing, leaving Africa as the third greatest net GHG sink (93 [134-36] Tg CO_2e $_2$ yr^{-1}), globally. Australasia and West Asia are moderate GHG sinks (both ~25 Tg CO_2e yr^{-1}), while in East and South Asia, coastal vegetation CO_2 sinks are largely offset by estuarine GHG release, resulting in a combined small net GHG sink of <20 Tg CO_2e yr^{-1}. In Europe and Russia, estuarine GHG outgassing across a large estuarine surface area exceeds uptake from the relatively small area of coastal vegetation, making these regions net GHG sources. As such, our regionalized assessment suggests that in addition to being a net global sink of GHGs for the atmosphere, the sink attributed to estuaries and coastal vegetation is also a common feature in many regions across the world.

The limitations of our GHG synthesis fall largely into four categories: mapping of ecosystems, GHG flux measurements, spatio-temporal variability, and coupling between coastal vegetation and estuaries. Tidal marsh area used in this study[29] is likely underestimated due to the recent surge in restoration efforts resulting in a gain in tidal marsh area[50] and the lack of global mapping of freshwater tidal marshes. We exclude low salinity (< 0.5) tidal river fluxes because of the difficulty to separate these from non-tidal rivers, and because the biogeochemistry and residence times are distinctly different from brackish estuaries[19]. Our coastal GHG budget is focused on the interface of the atmosphere with coastal vegetation and estuaries. We do not account for other radiative effects that may arise from lateral transport, such as offsite emissions, or 'blue carbon' burial in marine sediments. The ebullitive and plant-mediated CH_4 flux is underrepresented in our analysis due to the scarcity of such data. GHG flux measurements, despite recent progress, are still lacking, particularly from Africa, Russia, and West Asia. To better capture temporal variability, eddy covariance towers and conventional time-series measurements are needed, even in regions with good spatial coverage. High spatio-temporal variability means that techniques such as remote sensing[50], empirical modeling, and process-based modeling are needed for extrapolating flux densities and projecting future hotspots, particularly in the face of climate change and population growth along the coast. Coastal vegetation and estuaries are intimately coupled. However, the quantity and quality of material transported laterally and the fraction and mechanisms controlling outgassing through the coastal vegetation-estuary interface or further offshore are currently poorly known[51], particularly for CH_4 and N_2O. Despite its limitations, our coastal GHG synthesis addresses the current research gap between local and global scales and identifies regional hotspots. The future role of coastal ecosystems as a sink or source of GHGs in each world region will depend on the adoption of best practices to reduce CH_4 and N_2O emissions while strengthening the CO_2 uptake.

Methods:

Definitions of estuaries (tidal systems and deltas, lagoons, fjords) and coastal vegetation (mangroves, salt marshes, seagrasses) can be found in the Supplementary Information.

Estuarine surface areas

The estuarine surface areas used in this study were calculated using a novel regionalized approach that combines available national databases and an extrapolation method that derives the total estuarine surface area of a region from the surface areas of its largest systems[30]. Using a well-established global coastal segmentation comprising 45 regions (MARgins and CATchment Segmentation, (MARCATS)[10]), a surface area was determined for each estuary type (tidal systems and deltas, lagoons, or fjords) in each region. Wherever exhaustive regional or national databases were available and covered an entire MARCATS segment (i.e., Australia, New Zealand, and all lagoons surrounding the Mediterranean Sea), the type-specific surface areas were extracted from these databases by assigning each identified system to a given type. In other regions, the surface areas were extrapolated from the 5 to 10 largest systems. The extrapolation method relies on the observation that the cumulative estuarine surface area expressed as a function of the number of estuaries ranked by decreasing size within a sufficiently large stretch of coastline can be fitted by an equation of the form $S = (a * N) / (b + N)$ with S being the total estuarine surface area (in km^2), N, the number of estuaries and a and b dimensionless calibration coefficients. Using several extensive national estuarine databases (Australia, New Zealand, United States), it was shown that fitting the parameters of this generic formula using only the 10 largest estuaries of a given region generally allows predicting the total cumulative surface area of the region with a 9 % accuracy. This uncertainty due to extrapolation is complemented by an uncertainty associated with the accuracy in estimating the surface areas of the individual systems used to perform the calculations and which range from 4 to 15% depending on the estuarine type. Within each MARCATS, the surface areas of the 10 largest systems of each estuarine type were gathered from national databases (United Kingdom, Mexico, United States, Australia, South Africa, South Korea), regional surveys (FAO, UNESCO), global databases (Sea Around Us) or calculated individually using GIS. Those data were then sorted and fitted using the equation described above to derive the estuarine surface area for each MARCATS and each estuarine type, and finally summed to obtain the area for each of the ten RECCAP2 regions. For further details, see Laruelle et al.[30].

Coastal vegetation surface areas

For all three coastal vegetation types, we segmented the vegetation area given as a global collection of polygons[27–29] into the larger MARCATS regions[10] using the following approach: The MARCTAS regions were first converted from the raster format to polygons using the python package *rasterio*[52]. To find the area of each coastal vegetation type within a given MARCATS region we first dissolved overlapping individual polygons to avoid overestimation of the vegetation area. We found the union of each polygon and the larger MARCATS region and recalculated the area using the EPSG:6933 projection, using the python package *geopandas*[53], and finally summed these values. The same process was repeated for each large-scale MARCATS region and coastal vegetation type individually. The available shapefiles for MARCATS regions were converted from gridded outputs to polygons using *rasterio*[52]. Using *geopandas* for each region, we dissolved overlapping polygons and calculated the area of each polygon within the region using the EPSG:6933 projection, and finally summed the area for each of the ten RECCAP2 regions.

Estuarine greenhouse gas fluxes

We calculated estuary water-air fluxes of CO_2, CH_4 and N_2O based on data from peer-reviewed publications until the end of 2020. We conducted a literature search in Google Scholar and data publishers (Fluxnet, PANGAEA, MEMENTO, British Oceanographic Data Centre) using the search string '(CO_2 OR CH_4 OR N_2O) AND (tidal system OR delta OR lagoon OR fjord)'. Additionally, we scanned the reference lists of publications. For each site/study location (> 10 km apart), we averaged spatial and seasonal variation to a single water-air flux density, resulting in 204 sites for CO_2, 157 sites for CH_4 and 123 sites for N_2O, globally, which are 20%, 21% and 85% more sites compared to previous global syntheses for CO_2 [9], CH_4 [17], and N_2O [23], respectively. For estuary CH_4 estimates, we included primarily diffusive water-air fluxes (computed from the gas transfer velocity and the concentrations of CH_4 in water and air) and four studies using floating chamber incubations that estimate the total CH_4 flux (diffusive and ebullitive). The low number of total CH_4 flux estimates means that the ebullitive flux is underestimated in our analysis, particularly in the upper estuarine region. Each site/flux density was then distributed following the ten RECCAP2 regions using lat/long coordinates provided in the original studies or from Google Earth based on the study site description. Sites were categorised as either 'tidal systems and deltas', 'lagoons', or 'fjords' based on the authors' characterisation of their study site. In systems for which the site description was ambiguous or not detailed enough, the type was assigned following the hierarchical steps for estuarine type determination provided by Dürr et al.[31] which are based on hydrological, lithological, and morphological criteria. Estuary CO_2 and CH_4 emissions have not been modelled at global scales because of the lack of an existing spatially explicit global estuarine model designed to perform such a task. However, we supplemented the literature-derived empirical estuarine estimates of N_2O emissions with results from the spatially explicit global model from Maavara et al.[25]. These authors used a stochastic-mechanistic model representing generalized nitrogen dynamics for water body types directly connected to river networks worldwide to extract relationships predicting N_2O emissions from water residence times and total nitrogen (TN) yields (i.e., area-normalized loads) delivered to each estuary. The global TN loads were calculated using an approach inspired by Global-NEWS models[54], and spatially routed nitrogen through an inland water network joined to the estuaries accounted for in Dürr et al.[31]. Emissions factors were calculated using scenarios that reflect existing literature assumptions and datasets. The model was aggregated at a spatial resolution of 0.5 degrees, which is the same used by Dürr et al.[31] for their estuarine typology. Each watershed thus was assigned an estuarine type based on the type of the coastal cell in which the mouth of the watershed was located. Complete model details are available in Maavara et al.[25].

Coastal vegetation greenhouse gas fluxes

We conducted a literature search in Google Scholar and data publishers (Fluxnet, PANGAEA, MEMENTO, British Oceanographic Data Centre) until the end of 2020 using the search string '(CO_2 OR CH_4 OR N_2O) AND (mangroves OR salt marshes OR seagrasses)'. Additionally, we scanned the reference lists of publications. For each site/study location (> 10 km apart), we averaged spatial and seasonal variation to a single flux density, resulting in 37 sites for CO_2, 162 sites for CH_4 and 55 sites for N_2O in coastal vegetation (Extended Data Figure 3), which are 15% and 42% more sites compared to previous global syntheses of coastal wetlands for CH_4 [17] and N_2O [23], respectively. In our global synthesis, we use only long-term eddy-covariance (EC) CO_2 fluxes for coastal vegetation. We exclude chamber measurements as they do not provide information on CO_2 ecosystem exchange with a temporal coverage that is comparable to EC measurements. Although EC towers are still relatively rare in coastal vegetation, this method provides robust high-resolution long-term monthly, seasonal, and often annual data of net ecosystem exchange. EC measurements of CH_4 and N_2O are extremely rare in coastal vegetation. Therefore, we combined the few existing EC data with water-air, sediment-air, sediment-water, plant (leaf, root, stem)-air, and ebullition CH_4 or N_2O fluxes where available.

CO_2-equivalent greenhouse gas fluxes

For the purpose of directly comparing the relative radiative forcing effects of CO_2, CH_4, and N_2O to one another, we express GHG fluxes as CO_2-equivalents for the 20-year and 100-year time horizons using the global warming potential (GWP_{20} and GWP_{100}) including chemical adjustments reported in the Sixth Assessment Report of the Intergovernmental Panel on Climate Change[55]. For CH_4, we use the non-fossil GWP_{20} and GWP_{100}. Accordingly, over a 20-year time period, which is important for climate policies based on shorter timescales, 1 kg of CH_4 and N_2O have the same global warming potential as 79.9 kg or 273 kg of CO_2, respectively. Over a 100-year time period, 1 kg of CH_4 or N_2O have the same global warming potential as 27.0 kg or 273 kg of CO_2, respectively. The net contemporary GHG radiative balance for a given region, ecosystem, and time horizon is the sum of the CO_2-equivalents over the three gases.

Data analyses and upscaling

Data processing and statistical analyses were performed in R software[56]. A non-parametric bootstrapping method using the package *boot* in R was applied to resample flux densities for each of the 3 gases in each of the 6 ecosystems (3 estuary types and 3 coastal vegetation types) and in each of the 10 RECCAP2 regions (Extended Data Figure 4). The bootstrapping method used 1,000 iterations of the median of samples to produce a smoothed distribution of flux densities, and to generate a full set of statistics. Results from non-parametric bootstrapping were then multiplied by the corresponding surface area of each of the 6 ecosystem types in each of the 10 RECCAP2 regions. If an ecosystem type had less than three sites in a region, we applied the global statistics of this type in this region.

Uncertainty analysis

Uncertainties associated with flux densities were derived from the bootstrapping method that generated a full set of statistics including the first (Q1) and third (Q3) quartiles of the datasets.

For estuarine surface areas, the normality of the distribution was successfully tested and allowed deriving upper and lower 95% confidence intervals (c.i.) as well as the first (Q1) and third (Q3) quartiles from the standard deviation[30]. Global mangrove forest has been successfully mapped with an overall accuracy of 99% likelihood that the true value is between 93.6-94.5%[27]. The global extent of salt marshes is relatively uncertain with recent global estimates ranging from 55,000[28] to 90,800 km^2 [50]. Submerged seagrasses are challenging to map and current global estimates are highly uncertain. The most recent and continuously updated global seagrass mapping effort by UNEP-WCMC and Short[29] does not estimate uncertainty. Here, we assume an area per region uncertainty of 5%, 10%, and 20% for mangroves, salt marshes, and seagrasses, respectively, noting that these uncertainties could be substantially larger for the latter two types of coastal vegetation. We then combined the respective uncertainties of GHG flux densities with uncertainties of surface area of either estuaries or coastal vegetation using the 'Root Sum of the Squares' method, which calculates the square-root of the linear sum of the squared standard uncertainty components, treating the uncertainty contributors as statistically independent. We present the combined uncertainties of Q1 and Q3 in accordance with the median (Q2) in the main article, because this statistical set represents the most appropriate measure of the non-normally distributed GHG fluxes.

Data Availability:

All data included in this study are freely available (https://doi.org/10.6084/m9.figshare.22351267 and ref 57). Data may be used if cited appropriately.

Acknowledgments:

We would like to thank the RECCAP2 Scientific Committee and the Global Carbon Project that initiated this group effort: https://www.globalcarbonproject.org/reccap/index.htm. We thank Ameriflux site teams, who contributed annual NEE sums for their sites: E. Stuart-Haëntjens, B. Bergamaschi, L. Windham-Myers, A. Vázquez-Lule, R. Vargas, J. Shahan, P. Oikawa, P. Hawman, D. Mishra, R. Sanders-DeMott and P. Polsenaere. J.A.R. and T.M. acknowledge funding by the Hutchinson Postdoctoral Fellowship from the Yale Institute for Biospheric Studies at Yale University. I.F. acknowledges the NSF LTER program (OCE 1637630). R.G.N. acknowledges support from NASA's Carbon Cycle Science Program. G.G.L. is research associate of the F.R.S-FNRS at the Université Libre de Bruxelles. P.R. received financial support from BELSPO through the project ReCAP, which is part of the

Belgian research program FedTwin, from the European Union's Horizon 2020 research and innovation program ESM 2025 – Earth System Models for the Future (grant no. 101003536) project and from the FRS-FRNS PDR project T.0191.23. B.D.E. acknowledges support from ARC grants DP220100918, LP200200910 and LP190100271. W.-J.C. acknowledges supports from NOAA and NSF. J.J.M.B. acknowledges the computational resources provided by Princeton Institute for Computational Science and Engineering (PICSciE) which were used for the land segmentation. B.V.D. was supported by the Bundesministerium für Bildung und Forschung (BMBF) project "CARBOSTORE" (no. 03F0875A), and from the German Academic Exchange Service (DAAD) project "The Ocean's Alkalinity: Connecting geological and metabolic processes and time-scales" (no. 57429828).

Author Contribution Statement:

J.A.R. and P.R. conceived and designed the study. J.A.R. did the synthesis for CH_4 and N_2O in estuaries, and for CH_4 and N_2O in coastal vegetation. B.D.E. and H.W.B. helped with the synthesis for N_2O in estuaries and coastal vegetation. T.M. provided the mechanistic model for N_2O in estuaries. G.G.L. did the synthesis for CO_2 in estuaries. I.F. did the synthesis for CO_2 in salt marshes. B.V.D. did the synthesis for CO_2 in seagrasses. J.A.R. did the synthesis for CO_2 in mangroves. J.J.M.B. segmented the coastal vegetation surface area. G.G.L. segmented the estuarine surface area. J.A.R. produced the results and figures and wrote the original draft of the paper. All authors helped with the interpretation of the data and contributed to the review and editing of the paper.

Competing Interest Statement:

The authors declare no competing interests.

Table 1. Global estuary and coastal vegetation greenhouse gas fluxes. Global median [Q1-Q3] estuary (tidal systems and deltas, lagoons, fjords) and coastal vegetation (mangroves, salt marshes, seagrasses) CO_2, CH_4, N_2O, and CO_2-equivalent (CO_2e) greenhouse gas fluxes using the global warming potential for the 20-year (GWP_{20}) and 100-year (GWP_{100}) time periods. Estuary N_2O fluxes are also shown based on the mechanistic model (output) by Maavara et al.[25].

Ecosystem	CO_2 Tg CO_2 yr^{-1}	CH_4 Tg CH_4 yr^{-1}	CH_4 Tg CO_2e yr^{-1} GWP_{20}	CH_4 Tg CO_2e yr^{-1} GWP_{100}	N_2O Gg N_2O yr^{-1}	N_2O Tg CO_2e yr^{-1} GWP_{20} and GWP_{100}
Tidal systems and deltas	126.6 [89.9-175.5]	0.14 [0.11-0.23]	10.8 [8.66-18.1]	3.66 [2.94-6.13]	35.1 [23.6-48.4], (49.7)	9.58 [6.45-13.2]
Lagoons	50.0 [27.8-80.5]	0.11 [0.05-0.13]	8.53 [4.15-10.1]	2.89 [1.41-3.43]	9.93 [6.24-13.8], (14.1)	2.71 [1.70-3.76]
Fjords	-65.6 [-96.4- -23.5]	0.003 [0.002-0.008]	0.25 [0.15-0.62]	0.08 [0.05-0.21]	16.3 [11.8-20.6], (30.5)	4.46 [3.21-5.61]
Global estuaries	111.1 [72.7-170.3]	0.25 [0.07-0.46]	19.6 [5.45-36.9]	6.63 [1.85-12.5]	61.3 [41.4-93.8], (94.4)	16.8 [11.3-25.6]
Mangroves	-359.3 [-433.5- -333.4]	0.34 [0.21-0.50]	26.8 [16.4-39.8]	9.07 [5.57-13.5]	8.85 [4.36-19.3]	2.42 [1.19-5.27]
Salt marshes	-49.6 [-59.0- -41.2]	0.26 [0.14-0.36]	20.3 [11.2-28.3]	6.89 [3.80-9.60]	2.06 [-0.83-6.08]	0.56 [-0.23-1.66]
Seagrasses	-191.6 [-353.5- -53.2]	0.17 [0.09-0.21]	13.7 [7.04-16.9]	4.64 [2.38-5.73]	-4.56 [-5.98- -3.39]	-1.25 [-1.63- -0.93]
Global coastal vegetation	-600.6 [-773.5- -426.2]	0.77 [0.47-1.41]	60.8 [37.4-112.5]	20.6 [12.7-38.1]	6.35 [0.70-18.3]	1.73 [0.19-5.00]
Global estuaries + coastal vegetation	-489.5 [-700.8- -255.9]	1.01 [0.54-1.87]	80.4 [42.9-149.4]	27.2 [14.5-50.6]	67.7 [42.1-112.1]	18.5 [11.5-30.6]

Table 2. Regional coastal CO_2-equivalent greenhouse gas fluxes. Median [Q1-Q3] estuary and coastal vegetation CO_2-equivalents (CO_2e) greenhouse gas fluxes using the global warming potential for the 20-year (GWP_{20}) and 100-year (GWP_{100}) time periods. Negative values indicate net uptake of greenhouse gases from the atmosphere and positive values indicate net release of greenhouse gases to the atmosphere.

Region	Estuaries		Coastal vegetation		Estuaries + coastal vegetation	
	Tg CO_2e yr^{-1} (GWP_{20})	Tg CO_2e yr^{-1} (GWP_{100})	Tg CO_2e yr^{-1} (GWP_{20})	Tg CO_2e yr^{-1} (GWP_{100})	Tg CO_2e yr^{-1} (GWP_{20})	Tg CO_2e yr^{-1} (GWP_{100})
North America	-20.1 [-33.6- -5.97]	-25.7 [-33.9- -12.1]	-89.4 [-123.9- -43.0]	-102.0 [-131.2- -64.6]	-109.6 [-157.5- -49.0]	-127.7 [-165.1- -76.7]
South America	13.3 [7.68-26.1]	11.6 [6.54-22.7]	-48.5 [-66.1- -26.9]	-51.1 [-66.1- -32.8]	-35.3 [-58.4- -0.79]	-39.5 [-59.5- -10.1]
Europe	31.3 [28.5-36.2]	30.5 [27.9-34.9]	-14.5 [-19.5- -5.72]	-15.1 [-19.9- -6.46]	16.8 [8.98-30.5]	15.4 [8.07-28.5]
Africa	25.1 [13.4-44.9]	23.3 [13.4-37.3]	-110.5 [-143.4- -56.6]	-116.0 [-147.1- -73.4]	-85.4 [-130.0- -11.7]	-92.6 [-133.8- -36.1]
Russia	30.4 [25.7-41.8]	29.3 [25.4-38.2]	-3.77 [-6.08- -1.17]	-5.23 [-7.05- -3.04]	26.6 [19.6-40.6]	24.1 [18.3-35.2]
West Asia	1.02 [0.91-1.28]	0.97 [0.86-1.23]	-22.8 [-29.4- -12.7]	-23.5 [-29.8- -15.1]	-21.8 [-28.5- -11.4]	-22.5 [-28.9- -13.9]
East Asia	7.59 [6.24-10.4]	7.21 [6.03-9.80]	-10.1 [-18.0- -3.09]	-15.1 [-21.8- -9.81]	-2.51 [-11.8-7.27]	-7.88 [-15.8- -0.01]
South Asia	12.6 [10.6-13.9]	12.5 [10.5-13.8]	-21.5 [-30.7- -8.48]	-24.2 [-31.9- -13.5]	-8.93 [-20.1-5.47]	-11.7 [-21.4-0.34]
Southeast Asia	12.5 [7.97-21.4]	12.3 [7.78-21.2]	-164.9 [-229.2- -122.8]	-168.0 [-231.5- -127.0]	-152.4 [-221.2- -101.4]	-155.8 [-223.7- -105.8]
Australasia	33.7 [22.1-42.8]	32.5 [21.4-41.4]	-51.9 [-69.7- -28.2]	-58.0 [-74.3- -37.4]	-18.2 [-47.6-14.6]	-25.5 [-53.0-3.95]
Global	147.4 [89.5-232.8]	134.5 [85.9-208.4]	-538.0 [-735.9- -308.7]	-578.2 [-760.7- -383.1]	-390.6 [-646.5- -75.8]	-443.8 [-674.8- -174.6]

Figure Captions (main text):

Figure 1: Regional and global estuary GHG fluxes. The box-whisker plots show the median and interquartile (Q1-Q3) range of CO_2, CH_4, and N_2O fluxes in tidal systems and deltas (TD), lagoons (LA), fjords (FJ) in ten RECCAP2 regions and globally. A positive value indicates a flux from the ecosystem to the atmosphere and a negative value a flux from the atmosphere to the ecosystem. Outliers (open circles) are shown only for global plots. The asterisk (*) indicates that the flux was upscaled based on global statistics ($n < 3$) (see Methods).

Figure 2: Regional and global coastal vegetation GHG fluxes. The box-whisker plots show the median and interquartile (Q1-Q3) range of CO_2, CH_4, and N_2O fluxes in mangroves (MA), salt marshes (SM), and seagrasses (SE) in ten RECCAP2 regions and globally. A positive value indicates a flux from the ecosystem to the atmosphere (emission) and a negative value a flux from the atmosphere to the ecosystem (uptake). Outliers (open circles) are shown only for global plots. The asterisk (*) indicates that the flux was upscaled based on global statistics ($n < 3$) (see Methods)

Figure 3: **Global and regional coastal CO_2-equivalent GHG fluxes.** a) Global median GHG sources and sinks of estuaries and coastal vegetation using the global warming potential for the 20-year (GWP_{20}, top) and 100-year (GWP_{100}, bottom) time horizons. The radiative balance is expressed as CO_2-equivalents in Tg CO_2e yr^{-1} for CO_2, CH_4, N_2O, and their sum (net GHGs). b) Conceptual diagram showing the magnitude of the CO_2-equivalent GHG fluxes for estuaries, coastal vegetation, and their sum in the ten RECCAP2 regions and relative to each other. The size of the arrows is proportional to the fluxes in Tg CO_2e yr^{-1} (Table 2). The arrow size is the same for GWP_{20} and GWP_{100}, therefore arrows are not shown for the two GWP time horizons individually.

Figure 4: Estuary and coastal vegetation GHG fluxes in the land-to-ocean aquatic continuum (LOAC). a) the LOAC carbon loop model is adapted from Regnier et al.[5]. The green loop connects the terra-firme ecosystems to the open ocean. The two shorter loops connect the terra firme ecosystems to inland waters (grey) and the coastal vegetation, estuaries, and continental shelves to the open ocean (blue). F_{AW} refers to GHG fluxes by tidal wetlands (salt marshes and mangroves) and submerged vegetation and F_{EA} refers to estuarine GHG fluxes. b) Global median [Q1/Q3] CO_2-equivalent GHG fluxes using the global warming potential for the 20-year (GWP_{20}) and 100-year (GWP_{100}) time horizons in coastal vegetation and in estuaries. Here we include seagrasses in coastal vegetation fluxes (F_{AW}), whereas in Regnier et al.[5] seagrasses as submerged vegetation are separated from inter-tidal emergent mangroves and salt marshes. Units are in Tg CO_2e yr^{-1}.

References (main text):

1. IPCC, I. *Climate Change 2021: The Physical Science Basis. Contribution of Working Group I to the Sixth Assessment Report of the Intergovernmental Panel on Climate Change*. (2021).
2. Tian, H. *et al.* The terrestrial biosphere as a net source of greenhouse gases to the atmosphere. *Nature* **531**, 225–228 (2016).
3. Raymond, P. A. *et al.* Global carbon dioxide emissions from inland waters. *Nature* **503**, 355–359 (2013).
4. Zheng, Y. *et al.* Global methane and nitrous oxide emissions from inland waters and estuaries. *Glob. Chang. Biol.* 4713–4725 (2022).
5. Regnier, P., Resplandy, L., Najjar, R. G. & Ciais, P. The land-to-ocean loops of the global carbon cycle. *Nature* **603**, 401–410 (2022).
6. Abril, G. & Borges, A. V. Ideas and perspectives: Carbon leaks from flooded land: Do we need to replumb the inland water active pipe? *Biogeosciences* **16**, 769–784 (2019).
7. Cai, W.-J. Estuarine and Coastal Ocean Carbon Paradox: CO_2 Sinks or Sites of Terrestrial Carbon Incineration? *Ann. Rev. Mar. Sci.* **3**, 123–145 (2011).
8. Bauer, J. E. *et al.* The changing carbon cycle of the coastal ocean. *Nature* **504**, 61–70 (2013).
9. Chen, C. T. A. *et al.* Air-sea exchanges of CO_2 in the world's coastal seas. *Biogeosciences* **10**, 6509–6544 (2013).
10. Laruelle, G. G. *et al.* Global multi-scale segmentation of continental and coastal waters from the watersheds to the continental margins. *Hydrol. Earth Syst. Sci.* **17**, 2029–2051 (2013).
11. Macreadie, P. I. *et al.* Blue carbon as a natural climate solution. *Nat. Rev. Earth Environ.* **2**, 826–839 (2021).
12. Gattuso, J.-P., Williamson, P., Duarte, C. M. & Magnan, A. K. The Potential for Ocean-Based Climate Action: Negative Emissions Technologies and Beyond. *Front. Clim.* **2**, 1–8 (2021).
13. Rosentreter, J. A., Maher, D. T., Erler, D. V, Murray, R. H. & Eyre, B. D. Methane emissions partially offset "blue carbon" burial in mangroves. *Sci. Adv.* **4**, eaao4985 (2018).
14. Oreska, M. P. J. *et al.* The greenhouse gas offset potential from seagrass restoration. *Sci. Rep.* **10**, 7325 (2020).
15. Rosentreter, J. A., Al‐Haj, A. N., Fulweiler, R. W. & Williamson, P. Methane and Nitrous Oxide Emissions Complicate Coastal Blue Carbon Assessments. *Global Biogeochem. Cycles* **35**, 1–8 (2021).
16. Williamson, P. & Gattuso, J. Carbon Removal Using Coastal Blue Carbon Ecosystems Is Uncertain and Unreliable, With Questionable Climatic Cost-Effectiveness. *Front. Clim.* **4**, 1–14 (2022).
17. Rosentreter, J. A. *et al.* Half of global methane emissions come from highly variable aquatic ecosystem sources. *Nat. Geosci.* **14**, 225–230 (2021).
18. Al‐Haj, A. N. & Fulweiler, R. W. A synthesis of methane emissions from shallow vegetated coastal ecosystems. *Glob. Chang. Biol.* **26**, 2988–3005 (2020).
19. Borges, A. V. & Abril, G. Carbon Dioxide and Methane Dynamics in Estuaries. in *Treatise on Estuarine and Coastal Science* vol. 5 119–161 (Elsevier, 2011).
20. Maher, D. T., Sippo, J. Z., Tait, D. R., Holloway, C. & Santos, I. R. Pristine mangrove creek waters are a sink of nitrous oxide. *Sci. Rep.* **6**, 25701 (2016).
21. Murray, R., Erler, D., Rosentreter, J., Maher, D. & Eyre, B. A seasonal source and sink of nitrous oxide in mangroves: Insights from concentration, isotope, and isotopomer measurements. *Geochim. Cosmochim. Acta* **238**, 169–192 (2018).
22. De Wilde, H. P. J. & De Bie, M. J. M. Nitrous oxide in the Schelde estuary: Production by nitrification and emission to the atmosphere. *Mar. Chem.* **69**, 203–216 (2000).
23. Murray, R. H., Erler, D. V. & Eyre, B. D. Nitrous oxide fluxes in estuarine environments: response to global change. *Glob. Chang. Biol.* **21**, 3219–3245 (2015).
24. Kroeze, C., Dumont, E. & Seitzinger, S. Future trends in emissions of N_2O from rivers and estuaries. *J. Integr. Environ. Sci.* **7**, 71–78 (2010).
25. Maavara, T. *et al.* Nitrous oxide emissions from inland waters: Are IPCC estimates too high? *Glob. Chang. Biol.* **25**, 473–488 (2019).
26. Ciais, P. *et al.* Definitions and methods to estimate regional land carbon fluxes for the second

phase of the REgional Carbon Cycle Assessment and Processes Project (RECCAP-2). *Geosci. Model Dev. Discuss.* **2020**, 1–46 (2020).

27. Bunting, P. *et al.* The Global Mangrove Watch-A New 2010 Global Baseline of Mangrove Extent. *Remote Sens.* **10**, 1669 (2018).
28. Mcowen C, Weatherdon LV, Bochove J, Sullivan E, Blyth S, Zockler C, Stanwell-Smith D, Kingston N, Martin CS, Spalding M, Fletcher S (2017). A global map of saltmarshes (v6.1). Biodiversity Data Journal 5: e11764. Paper DOI: https://doi.org/10.3897/BDJ.5.e11764; Data DOI: https://doi.org/10.34892/07vk-ws51
29. UNEP-WCMC, Short FT (2017). Global distribution of seagrasses (version 6.0). Sixth update to the data layer used in Green and Short (2003). Cambridge (UK): UN Environment World Conservation Monitoring Centre. URL: http://data.unepwcmc.org/datasets/7.
30. Laruelle, G. G., Rosentreter, J. A., Regnier P. Extrapolation based regionalized re-evaluation of the global estuarine surface area. (preprint: https://doi.org/10.31223/X5X664).
31. Dürr, H. H. *et al.* Worldwide typology of nearshore coastal systems: defining the estuarine filter of river inputs to the oceans. *Estuaries and Coasts* **34**, 441–458 (2011).
32. Woodwell, G. M., Rich, P. H. & Hall, C. A. S. Carbon in estuaries. in *Carbon and the Biosphere* (eds. Woodwell, G. M. & Pecan, E. V) 221–240 (Technical Information Center, U.S. Atomic Energy Commission, National Technical Information Service, 1973).
33. Stewart, B. T., Santos, I. R., Tait, D. R., Macklin, P. A. & Maher, D. T. Submarine groundwater discharge and associated fluxes of alkalinity and dissolved carbon into Moreton Bay (Australia) estimated via radium isotopes. *Mar. Chem.* **174**, 1–12 (2015).
34. Borges, A. V. *et al.* Variability of the gas transfer velocity of CO_2 in a macrotidal estuary (the Scheldt). *Estuaries* **27**, 593–603 (2004).
35. Frankignoulle, M. Carbon Dioxide Emission from European Estuaries. *Science* **282**, 434–436 (1998).
36. Regnier, P. *et al.* Modelling Estuarine Biogeochemical Dynamics: From the Local to the Global Scale. *Aquat. Geochemistry* **19**, 591–626 (2013).
37. Lovelock, C. E. & Reef, R. Variable Impacts of Climate Change on Blue Carbon. *One Earth* **3**, 195–211 (2020).
38. Alongi, D. M. Carbon Cycling and Storage in Mangrove Forests. *Ann. Rev. Mar. Sci.* **6**, 195–219 (2014).
39. Alongi, D. M. Carbon Balance in Salt Marsh and Mangrove Ecosystems: A Global Synthesis. *J. Mar. Sci. Eng.* **8**, 767 (2020).
40. Bange, H. W., Bartell, U. H., Rapsomanikis, S. & Andreae, M. O. Methane in the Baltic and North Seas and a reassessment of the marine emissions of methane. *Global Biogeochem. Cycles* **8**, 465–480 (1994).
41. Gelesh, L., Marshall, K., Boicourt, W. & Lapham, L. Methane concentrations increase in bottom waters during summertime anoxia in the highly eutrophic estuary, Chesapeake Bay, U.S.A. *Limnol. Oceanogr.* **61**, S253–S266 (2016).
42. Koné, Y. J. M., Abril, G., Delille, B. & Borges, A. V. Seasonal variability of methane in the rivers and lagoons of Ivory Coast (West Africa). *Biogeochemistry* **100**, 21–37 (2010).
43. Donato, D. C. *et al.* Mangroves among the most carbon-rich forests in the tropics. *Nat. Geosci.* **4**, 293–297 (2011).
44. Maher, D. T., Santos, I. R., Golsby-Smith, L., Gleeson, J. & Eyre, B. D. Groundwater-derived dissolved inorganic and organic carbon exports from a mangrove tidal creek: The missing mangrove carbon sink? *Limnol. Oceanogr.* **58**, 475–488 (2013).
45. Rao, G. D. & Sarma, V. V. S. S. Variability in Concentrations and Fluxes of Methane in the Indian Estuaries. *Estuaries and Coasts* **39**, 1639–1650 (2016).
46. Bange, H. W., Rapsomanikis, S. & Andreae, M. O. The Aegean Sea as a source of atmospheric nitrous oxide and methane. *Mar. Chem.* **53**, 41–49 (1996).
47. Chmura, G. L., Kellman, L., van Ardenne, L. & Guntenspergen, G. R. Greenhouse Gas Fluxes from Salt Marshes Exposed to Chronic Nutrient Enrichment. *PLoS One* **11**, e0149937 (2016).
48. Dausse, A. *et al.* Biogeochemical functioning of grazed estuarine tidal marshes along a salinity gradient. *Estuar. Coast. Shelf Sci.* **100**, 83–92 (2012).
49. Chen, J., Wells, N. S., Erler, D. V. & Eyre, B. D. Land-Use Intensity Increases Benthic N_2O

Emissions Across Three Sub-Tropical Estuaries. *J. Geophys. Res. Biogeosciences* **127**, 1–15 (2022).

50. Murray, N. J. *et al.* High-resolution mapping of losses and gains of Earth's tidal wetlands. *Science* **376**, 744–749 (2022).
51. Shields, M. R. *et al.* Carbon storage in the Mississippi River delta enhanced by environmental engineering. *Nat. Geosci.* **10**, 846–851 (2017).

References (methods):

52. Gillies, S., Ward, B., & Petersen, A. S. (2013). Rasterio: Geospatial raster I/O for Python programmers. URL https://github. com/mapbox/rasterio
53. Jordahl, K. *et al.* (2020). geopandas/geopandas: v0.8.1 (v0.8.1). Zenodo. URL https://doi.org/10.5281/zenodo.3946761
54. Mayorga, E. *et al.* Global Nutrient Export from WaterSheds 2 (NEWS 2): Model development and implementation. *Environ. Model. Softw.* **25**, 837–853 (2010).
55. Forster, P., T. Storelvmo, K. Armour, W. Collins, J.-L. Dufresne, D. Frame, D.J. Lunt, T. Mauritsen, M.D. Palmer, M. Watanabe, M. Wild, and H. Zhang. The Earth's Energy Budget, Climate Feedbacks, and Climate Sensitivity. In Climate Change 2021: The Physical Science Basis. Contribution of Working Group I to the Sixth Assessment Report of the Intergovernmental Panel on Climate Change [Masson-Delmotte, V., P. Zhai, A. Pirani, S.L. Connors, C. Péan, S. Berger, N. Caud, Y. Chen, L. Goldfarb, M.I. Gomis, M. Huang, K. Leitzell, E. Lonnoy, J.B.R. Matthews, T.K. Maycock, T. Waterfield, O. Yelekçi, R. Yu, and B. Zhou (eds.)]. Cambridge University Press, Cambridge, United Kingdom and New York, NY, USA, pp. 923–1054 (2021).
56. R Core Team (2020). R: A language and environment for statistical computing. R Foundation for Statistical Computing, Vienna, Austria. URL https://www.R-project.org/. (2020).
57. Rosentreter, J. *et al.* (2023): Coastal GHG data base. figshare. Dataset. https://doi.org/10.6084/m9.figshare.22351267

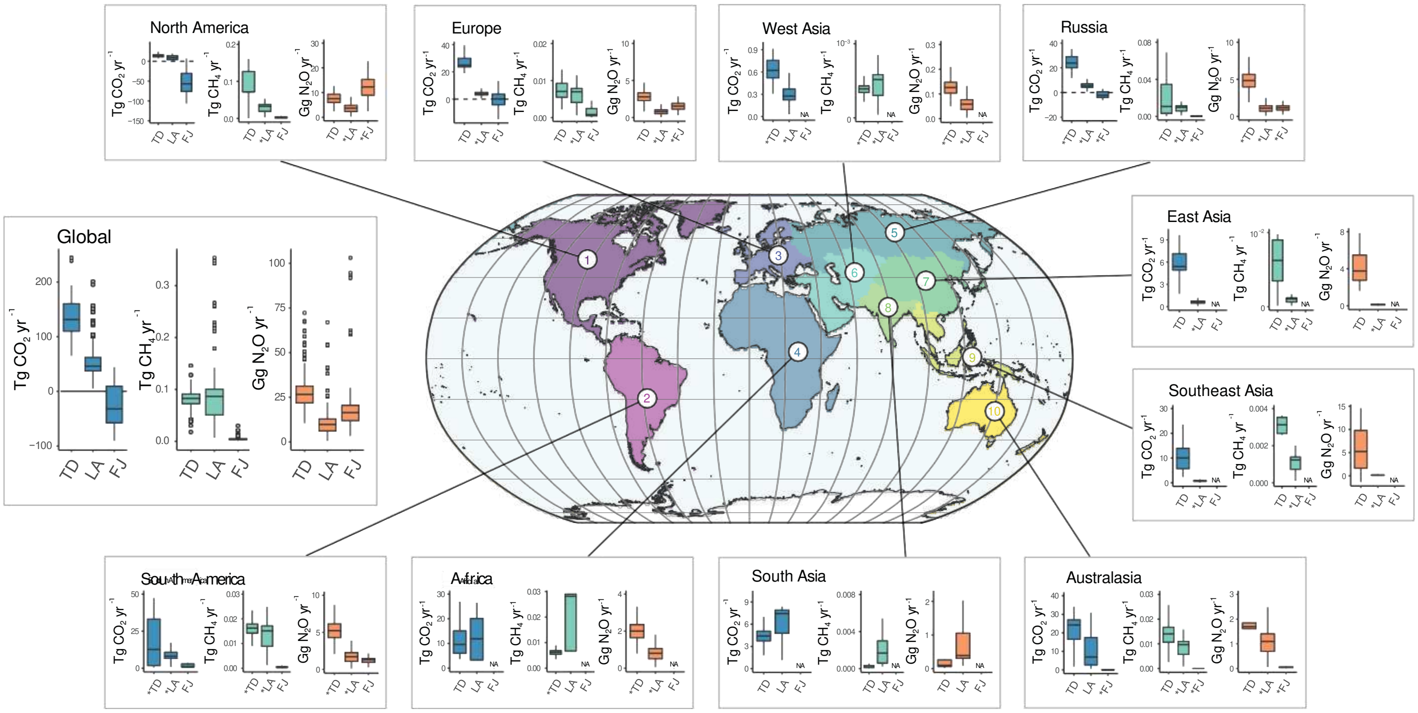

North America
Europe
West Asia
Russia
East Asia
Southeast Asia
Global
South America
Africa
South Asia
Australasia
Tg CO2 yr-1
Tg CH4 yr-1
Gg N2O yr-1
TD
LA
FJ
NA
1
2
3
4
5
6
7
8
9
10

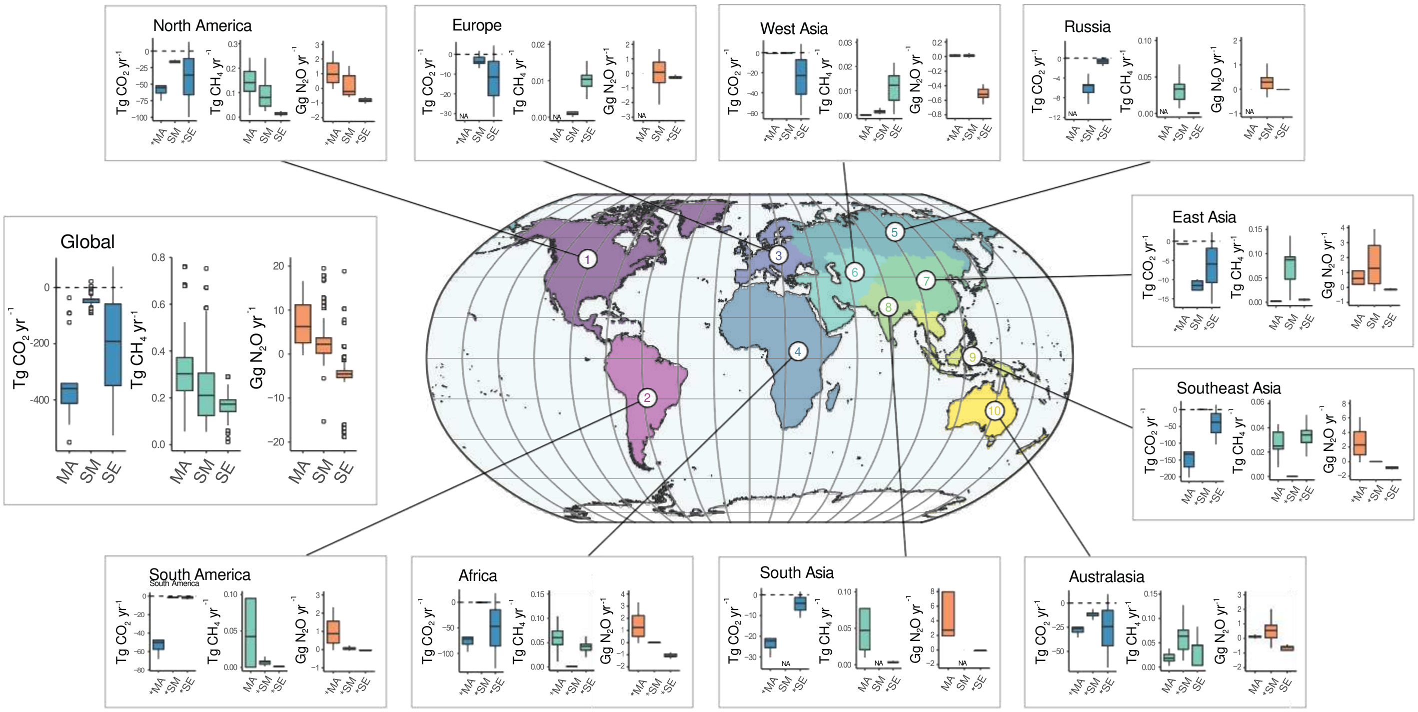

North America
Europe
West Asia
Russia
Global
East Asia
Southeast Asia
South America
Africa
South Asia
Australasia
Tg CO2 yr-1
Tg CH4 yr-1
Gg N2O yr-1
MA
SM
SE
NA
1
2
3
4
5
6
7
8
9
10

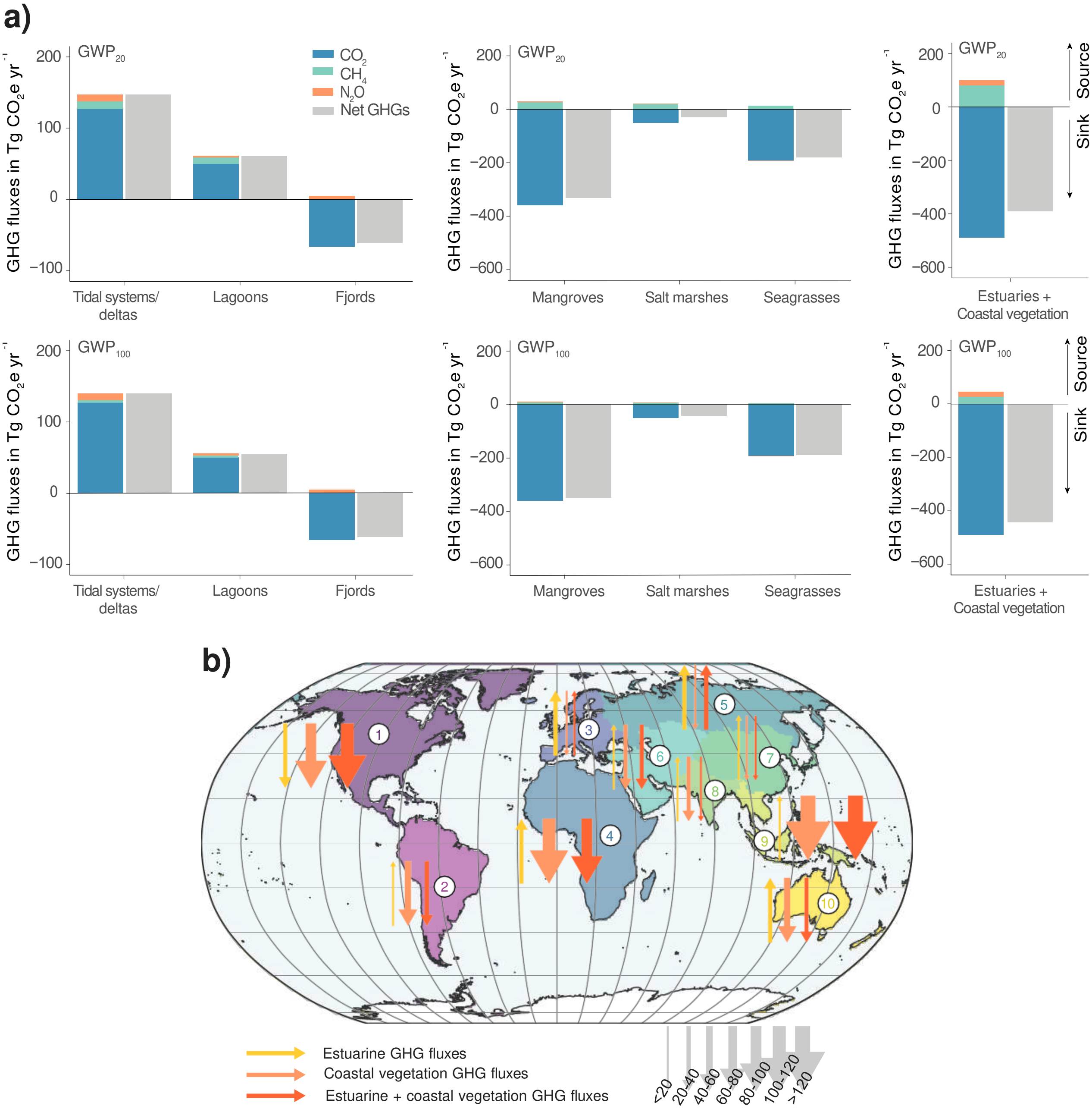

a)
GWP20
GWP100
CO2
CH4
N2O
Net GHGs
GHG fluxes in Tg CO2e yr-1
Tidal systems/ deltas
Lagoons
Fjords
Mangroves
Salt marshes
Seagrasses
Estuaries + Coastal vegetation
Source
Sink
b)
Estuarine GHG fluxes
Coastal vegetation GHG fluxes
Estuarine + coastal vegetation GHG fluxes
<20
20-40
40-60
60-80
80-100
100-120
>120

a)

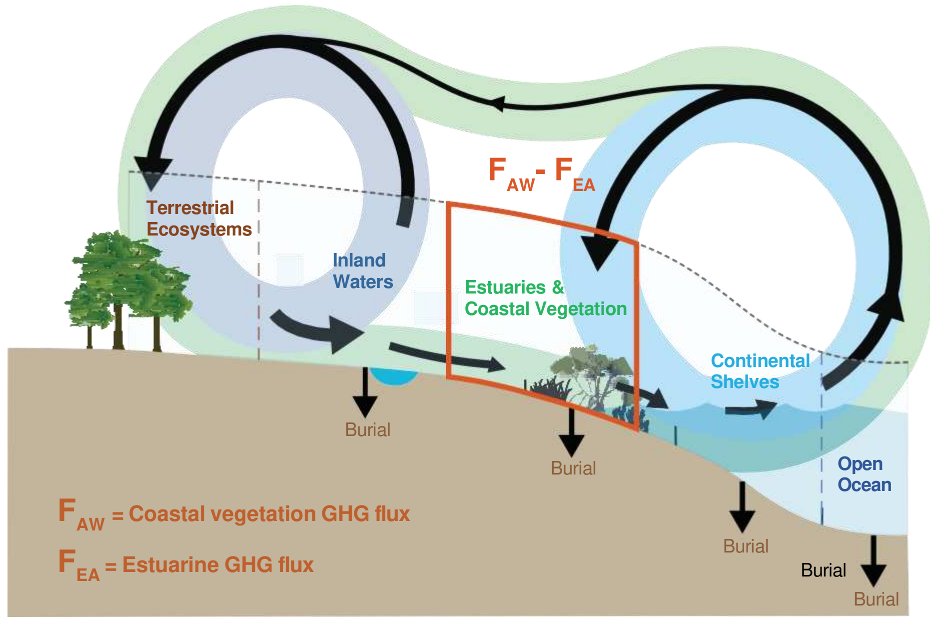

F_{AW} - F_{EA}
Terrestrial Ecosystems
Inland Waters
Estuaries & Coastal Vegetation
Continental Shelves
Open Ocean
Burial
Burial
Burial
Burial
Burial
F_{AW} = Coastal vegetation GHG flux
F_{EA} = Estuarine GHG flux

b)

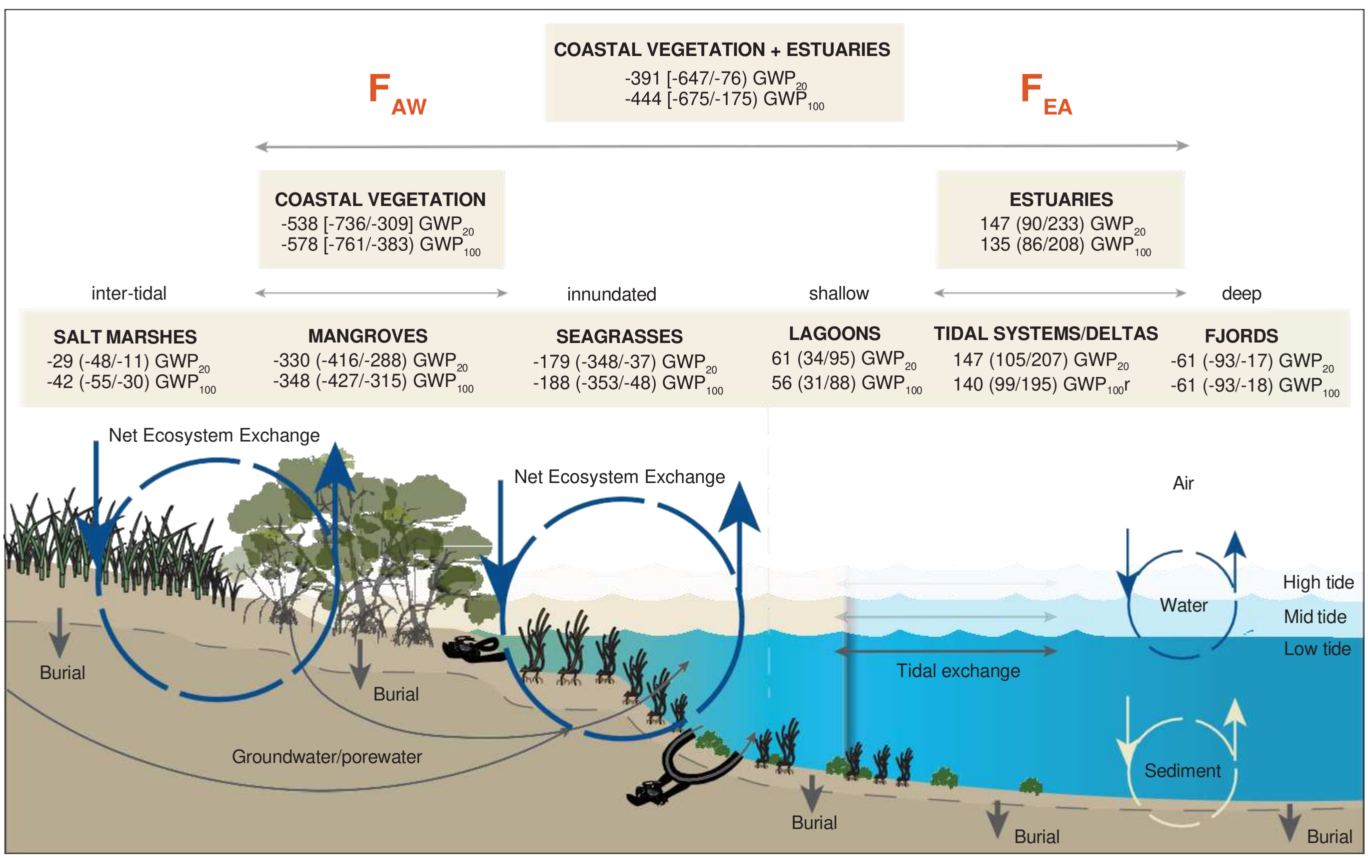

COASTAL VEGETATION + ESTUARIES
-391 [-647/-76) GWP_{20}
-444 [-675/-175) GWP_{100}
F_{AW}
F_{EA}
COASTAL VEGETATION
-538 [-736/-309] GWP_{20}
-578 [-761/-383) GWP_{100}
ESTUARIES
147 (90/233) GWP_{20}
135 (86/208) GWP_{100}
inter-tidal
innundated
shallow
deep
SALT MARSHES
-29 (-48/-11) GWP_{20}
-42 (-55/-30) GWP_{100}
MANGROVES
-330 (-416/-288) GWP_{20}
-348 (-427/-315) GWP_{100}
SEAGRASSES
-179 (-348/-37) GWP_{20}
-188 (-353/-48) GWP_{100}
LAGOONS
61 (34/95) GWP_{20}
56 (31/88) GWP_{100}
TIDAL SYSTEMS/DELTAS
147 (105/207) GWP_{20}
140 (99/195) GWP_{100}r
FJORDS
-61 (-93/-17) GWP_{20}
-61 (-93/-18) GWP_{100}
Net Ecosystem Exchange
Net Ecosystem Exchange
Air
High tide
Water
Mid tide
Low tide
Tidal exchange
Sediment
Burial
Burial
Groundwater/porewater
Burial
Burial
Burial

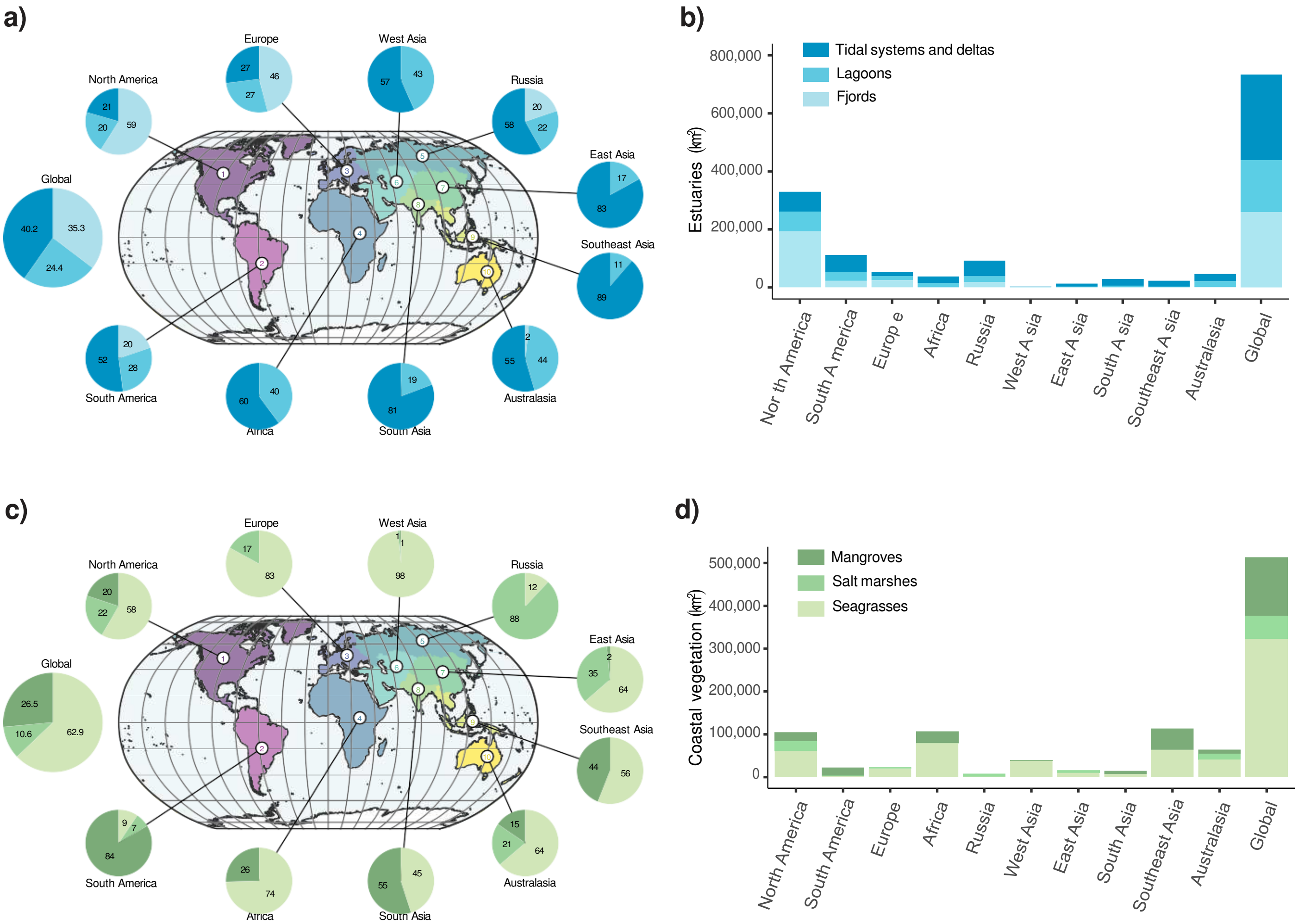

a)
Europe
West Asia
North America
Russia
Global
East Asia
Southeast Asia
South America
Africa
South Asia
Australasia
b)
Tidal systems and deltas
Lagoons
Fjords
Estuaries (km²)
800,000
600,000
400,000
200,000
0
Nor th America
South A merica
Europ e
Africa
Russia
West A sia
East A sia
South A sia
Southeast A sia
Australasia
Global
c)
d)
Mangroves
Salt marshes
Seagrasses
Coastal vegetation (km²)
500,000
400,000
300,000
200,000
100,000
0
North America
South America
Europe
Africa
Russia
West Asia
East Asia
South Asia
Southeast Asia
Australasia
Global

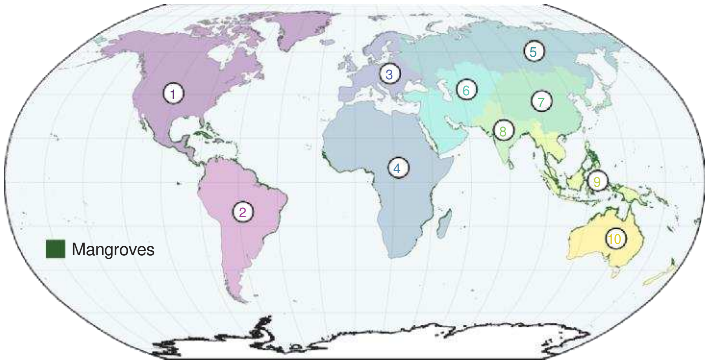

Mangrove forest	(km^2)
1 North America	= 20,910
2 South America	= 18,990
3 Europe	= 0
4 Africa	= 27,086
5 Russia	= 0
6 West Asia	= 267
7 East Asia	= 243
8 South Asia	= 8,402
9 Southeast Asia	= 49,967
10 Australasia	= 9,948

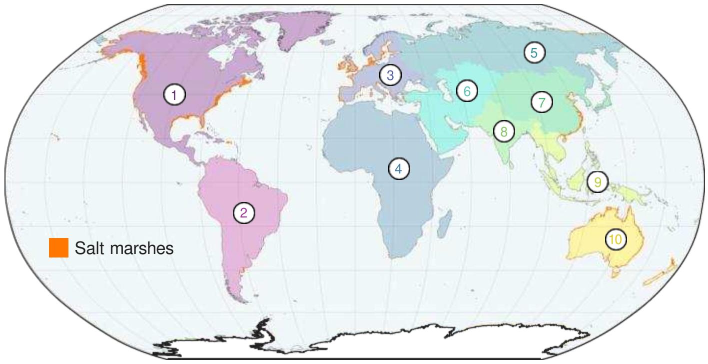

Salt marshes	(km^2)
1 North America	= 22,672
2 South America	= 1,564
3 Europe	= 3,975
4 Africa	= 119
5 Russia	= 7,044
6 West Asia	= 318
7 East Asia	= 5,475
8 South Asia	= 0
9 Southeast Asia	= 0.1
10 Australasia	= 13,383

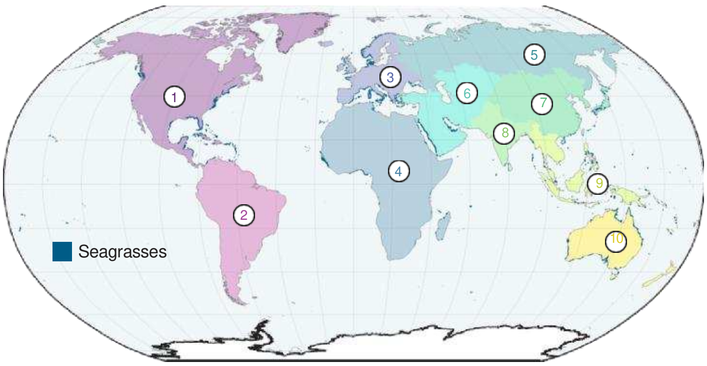

Seagrass meadows	(km^2)
1 North America	= 61,110
2 South America	= 2,136
3 Europe	= 19,365
4 Africa	= 79,201
5 Russia	= 961
6 West Asia	= 38,352
7 East Asia	= 9,984
8 South Asia	= 6,873
9 Southeast Asia	= 63,631
10 Australasia	= 41,009

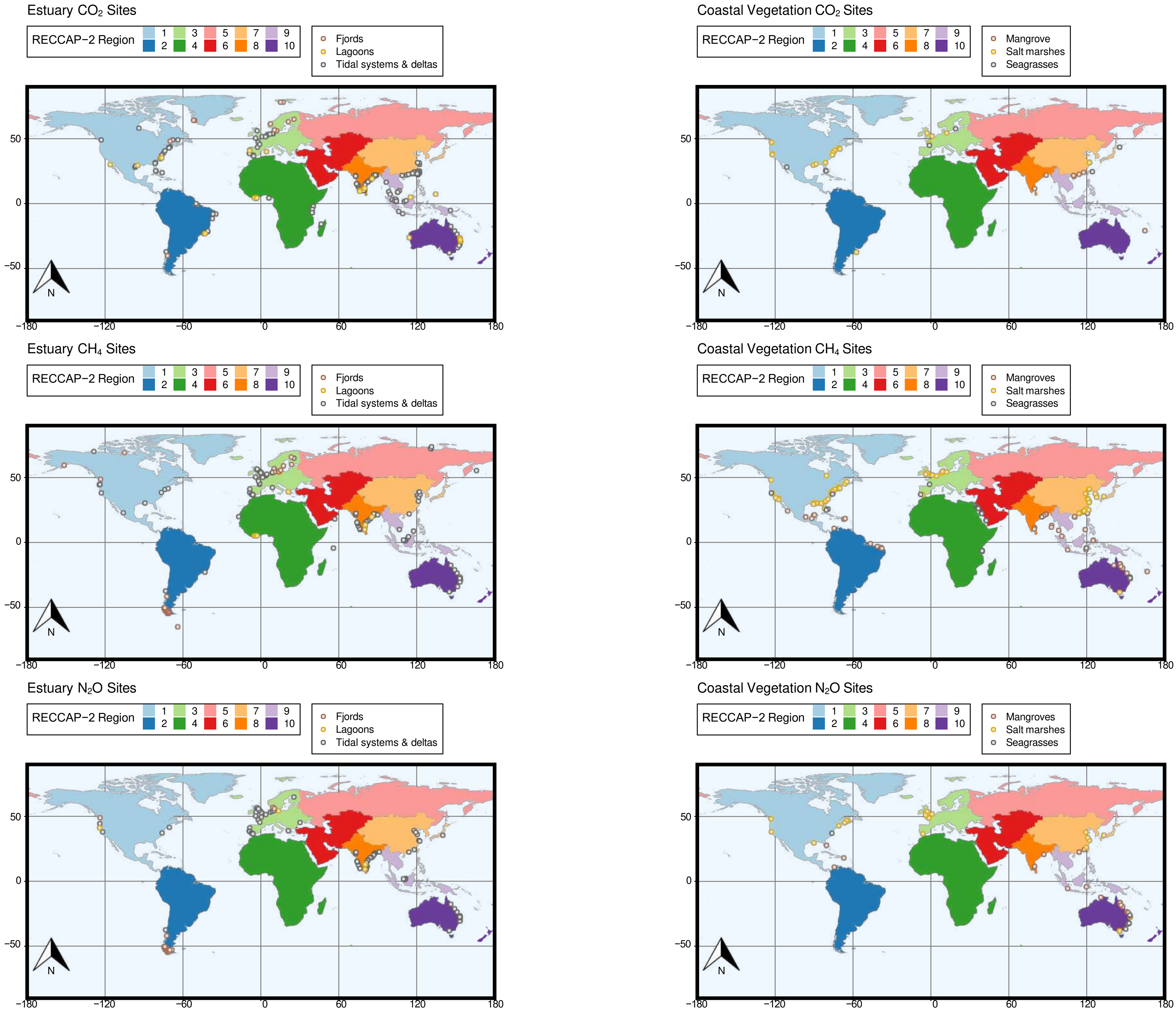

Estuary CO_2 Sites
RECCAP−2 Region
1 2 3 4 5 6 7 8 9 10
Fjords
Lagoons
Tidal systems & deltas
Coastal Vegetation CO_2 Sites
Mangrove
Salt marshes
Seagrasses
Estuary CH_4 Sites
Coastal Vegetation CH_4 Sites
Mangroves
Estuary N_2O Sites
Coastal Vegetation N_2O Sites
N
50
0
−50
−180
−120
−60
0
60
120
180

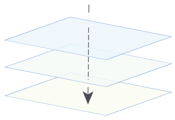
Level 1 - Greenhouse gas (CO_2, CH_4, N_2O) x3
Level 2 - Estuary type (tidal systems and deltas, lagoons, fjords) x3 OR
Coastal vegetation type (mangroves, salt marshes, seagrasses) x3
Level 3 - RECCAP2 region x10